Indian Journal of Pure & Applied Physics
Vol. 63, September 2025, pp. 796-802
DOI: 10.56042/ijpap.v63i9.14347

Dual Fano-type Resonance Based Refractive Index Sensor using 2D Silicon Photonic Crystal Waveguide-Cavity System

Nilaksha Ghosh & Sarang Medhekar*

Department of Physics, Central University of Jharkhand, Ranchi 835 222, India

Received: 12th Oct 2024; accepted:29th May 2025

In the present paper we have proposed a refractive index sensor created on the platform of a two-dimensional photonic crystal. The proposed device is based on dual Fano-type (asymmetric) resonance which is evident from the obtained spectral response with two peaks, one very sharp, while, the other very broad. The plane wave expansion method is used to calculate the band structure of the sensor and the two-dimensional finite difference time domain method is used to analyse the performance of the sensor. The band diagram shows that the structure allows only TE wave propagation. The sensitivity of the proposed sensor has been gauged by varying the background refractive index insteps of 0.01 within the range of 1.00-1.04 and found to be $1210 nm/RIU$. The quality factor and the figure of merit are found to be 2000.5 and 600 RIU^{-1} respectively. The broad peak exhibits larger redshift compared to the sharp peak with variation in background refractive-index. The sensor is compact in size allowing for its on-chip implementation.

Keywords: Photonic Crystal, Plane wave expansion method, Finite difference time domain method, Fano resonance, Refractive index sensing

1 Introduction

During the last decade, a lot of research efforts were focused on optical communication and sensing. Photonic crystals (PCs) in this context have emerged as the potential candidate mainly due to their extraordinary light guiding and manipulating capability[1]. PCs are nano structures with periodically varying refractive index (RI) in one, two or three dimensions and accordingly, classified as one, two or three dimensional PCs. PCs can prohibit propagation of a range of frequencies called photonic bandgap (PBG)[2]. By creating defects in the PC structures, electromagnetic waves of frequencies lying in the PBG region can be guided along the defects. Numerous proposals for PC based devices, e.g., optical transistors, logic gates, sensors etc. can be found in literature[3-8]. PC based RI sensors are at the focus of recent research explorations due to their potential applications in the areas ranging from structural health monitoring to bio-sensing[9-14]. This kind of sensors exhibit a high degree of sensitivity and accuracy compared to the traditional sensors.

Recently, there has been a lot of interest in the phenomenon of Fano (and Fano-type) resonance in optical systems mainly due to their applications in a wide area that includes sensing and switching[15-20]. Fano resonance originates due to the interference of discreet states (narrow resonances) with continuum (broad spectrum). In the proposed sensor, the cavity provides the discreet states and the waveguide provides a broad spectrum. Fano and Fano-type resonances are very sensitive to minute changes in the surrounding environment making those very useful for sensing purpose. The phenomenon (Fano and Fano-type resonance) has widely been studied, particularly for

(i) RI sensing in PC based structures/sensors,
(ii) Plasmonics
(iii) Meta surface based systems[21-29].

In recent times Harhouz *et.al*. studied Fano resonance and its application to RI sensing in 2D-PC based waveguide-cavity system[30]. Wu *et.al*. studied Fano resonance based temperature sensing in 2D PC slab structure[31]. Recently Agrawal *et.al*. designed a dual Fano resonance based RI sensor using dielectric meta surface[32].

In the present work we have designed a Fano resonance based RI sensor exhibiting dual Fano-type resonance on a photonic crystal platform. Our simulations show adequate redshift in the whole spectral response even for a very small change in the

*Corresponding author: E-mail: sarang.medhekar@cuj.ac.in

background RI and hence, RI of the background could be sensed with high sensitivity. The proposed sensor shows sensitivity (S) of $1210nm/RIU$ and a Quality factor (Q) of 2000.5. The Figure of merit (FOM) of the designed sensor is $600RIU^{-1}$.

The functioning of a RI sensor is straightforward, a measure and gets filled-in the empty space between rods of the sensor structure, changes the background RI, and hence, detected/measured. A RI sensor has numerous potential applications in fields like biological analysis, environmental monitoring, and drug analysis. RI sensors can be implemented in analyzing samples purity, detecting changes in the environment, and identifying biological analytes. RI sensor structures with higher and higher sensitivity is therefore always desirable.

2 Device Structure and Simulations

As in Fig. 1 (a), a 2D-PC basic platform of periodic arrays of 19*12 silicon (Si) rods in square lattice with air as the background material has been considered here. The structure allows for very high level of light confinement owing to high RI contrast. The lattice constant (a) is 0.62μm and the radius of the rods (r) is 0.09μm. The periodic variation of RI along the XZ direction allows for localization of light in XZ direction. As shown in Fig. 1 (b), the sensor structure consists of two defect waveguides (input and output waveguides) created by removing the Si rods. A cavity is placed between the input and output waveguides as shown. The cavity is consisting of five Si rods which are labelled as r_a (black), r_b (green), r_c (yellow) and r_d (blue) Rods r_a and r_b are the scattering rods and the cavity acts as a partially transmitting element (PTE). The input waveguide provides a continuum, while the cavity provides the discrete states. A schematic 3-D view of the sensor structure is shown in Fig. 1(c)

The plane wave expansion method (PWE) is used to calculate the band structure of the device[31] which is obtained as shown in Fig. 2. From the Fig. 2 it is clear that the considered device allows for propagation of TE waves only. Further, the structure exhibits only one PBG in the frequency range $0.346 \leq a/\lambda \leq 0.435$. The 2-D finite difference time domain (2D-FDTD) method was used to examine the propagation of electro-magnetic waves in the structure and to gauge the performance of the device. In order to avoid

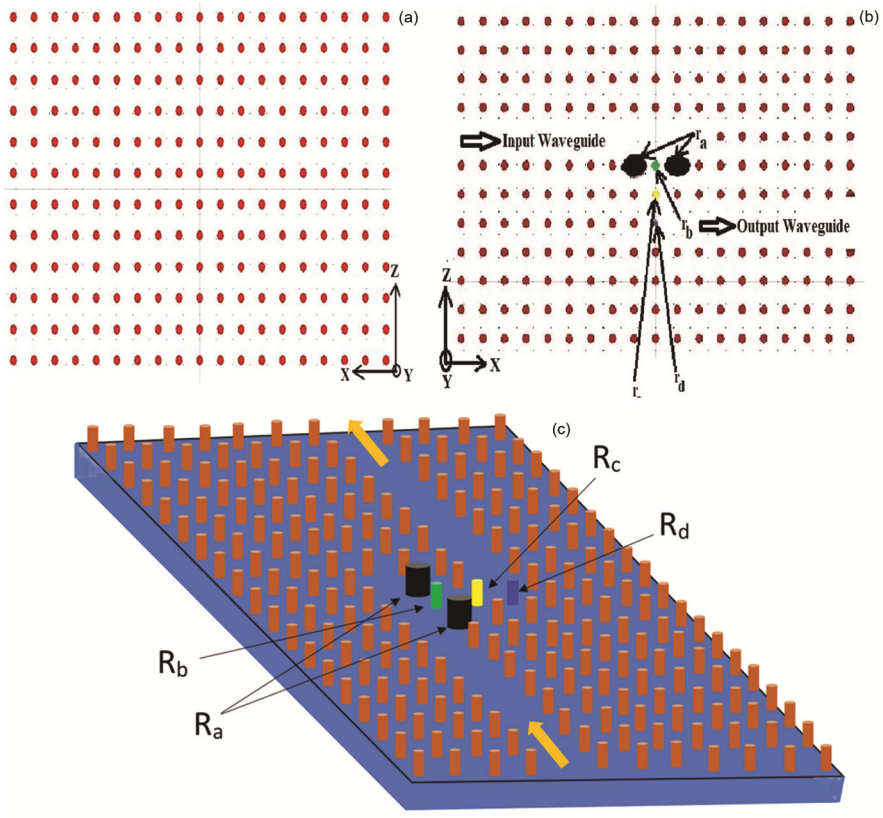

Fig. 1 — (a) Basic PC platform of the structure (b) Schematic diagram of the sensor structure(c) Schematic 3-Dview of the sensor

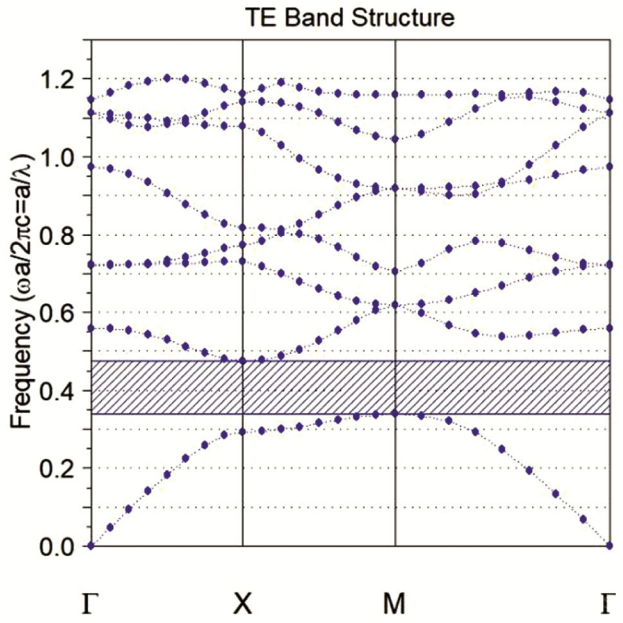

Fig. 2 — Band Diagram of the basic PC structure

the problem of back reflection, a perfectly match layer (PML) of 500nm was implemented[31]. The simulations were performed using the RSOFT-CAD software. As no propagation takes place in the Y-direction ($\partial/\partial y = 0$), components E_x,H_x,H_z are taken into account for the 2DFDTD simulations. The 2DFDTD formulae can be written as-

$$E_y|_{i-\frac{1}{2},k+\frac{1}{2}}^{n+\frac{1}{2}} = \left(\frac{2\Delta t}{2\varepsilon+\sigma\Delta t}\right)\left(\frac{H_x|_{i-\frac{1}{2},k+1}^{n} - H_x|_{i-\frac{1}{2},k}^{n}}{\Delta z} - Hz|i,k+12n - Hz|i-1,k+12n\Delta x + 2\varepsilon - \sigma\Delta t 2\varepsilon + \sigma\Delta t Ey|i-12,k+1\ 2n-12\right) \quad ...(1)$$

$$H_x|_{i-\frac{1}{2},k+\frac{1}{2}}^{n+1} = \left(\frac{2\Delta t}{2\mu+\rho\Delta t}\right)\left(\frac{E_y|_{i-\frac{1}{2},k+\frac{3}{2}}^{n+\frac{1}{2}} - E_y|_{i-\frac{1}{2},k+\frac{1}{2}}^{n+\frac{1}{2}}}{\Delta z}\right) + \left(\frac{2\mu-\rho\Delta t}{2\mu+\rho\Delta t}\right)H_z|_{i-\frac{1}{2},k+\frac{1}{2}}^{n} \quad \ldots (2)$$

$$H_z|_{i,k+\frac{1}{2}}^{n+\frac{1}{2}} = -\left(\frac{2\Delta t}{2\mu+\rho\Delta t}\right)\left(\frac{E_y|_{i+\frac{1}{2},k+\frac{1}{2}}^{n+\frac{1}{2}} - E_y|_{i-\frac{1}{2},k+\frac{1}{2}}^{n+\frac{1}{2}}}{\Delta x}\right) + \left(\frac{2\mu-\rho\Delta t}{2\mu-\rho\Delta t}\right)H_z|_{i,k+\frac{1}{2}}^{n} \quad \ldots (3)$$

Here *i* and *k* denotes the grid point lying in the *X-Z* plane and the discreet time steps are denoted by *n*. *Δx* and *Δz* are the gap between two consecutive grids and *Δt is* the time interval. The permittivity, permeability,

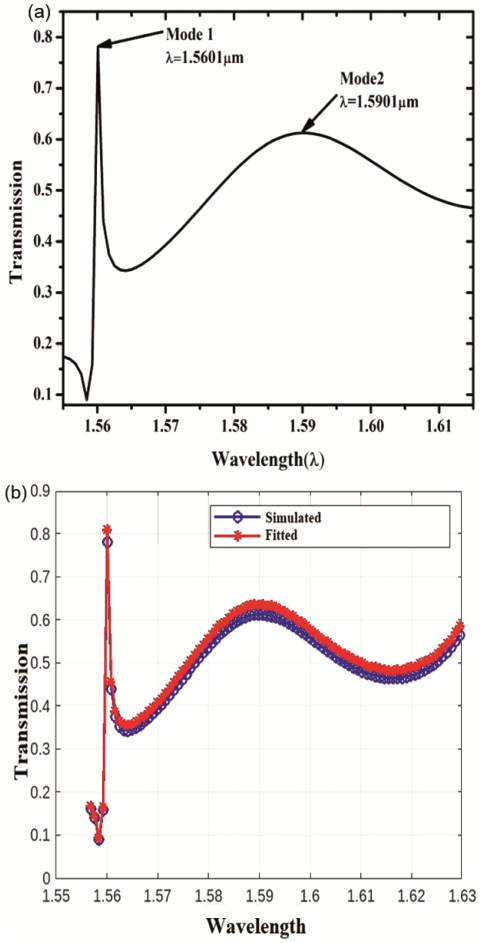

Fig. 3 — (a) Spectral response of the device (b) Simulated and fitted spectral response

electric conductivity and equivalent magnetic conductivity of the material are denoted by the symbols ε, μ, σ, ρ respectively. A grid size of $a/20 = 31nm$ has been considered.

A wide spectrum optical input is launched into the device and its spectral response is obtained. The background RI of the device was varied in the range of 1.00-1.04 in steps of 0.01 and the variation in the spectral response is noted. The proposed sensor shows redshift in its spectral response with increasing RI. Different parameters like the S, Q, FOM and limit of detection (LOD) of the sensor are calculated using the data generated from variation of spectral response with change in the background RI.

3 Results and Discussions

3.1 The Spectral Responses

From the spectral response of the device Fig. 3 (a) it can be seen that the proposed device exhibits a dual

Fano-type (asymmetric) resonance. The spectral response consists of a sharp resonance peak of high Q (=2000.5) followed by a broad peak of low Q (=53.30). The transmission spectrum is fitted using the formula

$$T_{Fano} = \left| a_1 + ia_2 + \frac{b}{\omega - \omega_0 + i\Upsilon} \right|^2 \quad \ldots (4)$$

Here a_1, a_2 and b denotes constant real numbers, ω_0 is the central frequency and Υ denotes the rate of damping of the resonance.

Figure 3 (b) shows the fitted spectral response. The Fig. 4 shows the difference in the spectral response with and without the cavity wherein, absence of the Fano-type resonance without the cavity can clearly be seen. The Fig. 5 (a-b) shows the propagation of light of wavelength 1.5601μm and 1.5901μm through the device.

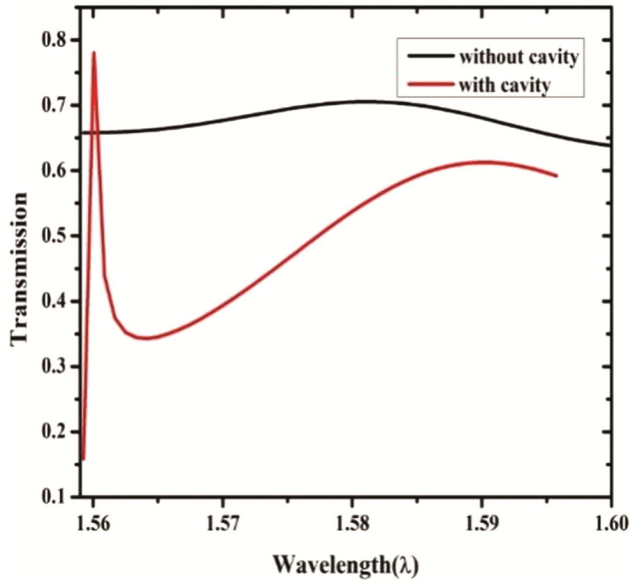

Fig. 4 — Spectral response of the device with and Without cavity

3.2 Optimization of the Structural Parameters

The structural parameters of the device are carefully studied in detail. Spectral responses of the device for different lattice constants is shown in Fig. 6 (a).Value of Q for different lattice constant is shown in Fig. 6(b).

Figure 6 (a-b) show that when the lattice constant is 0.62μm, the device exhibits maximum Q and also the maximum difference in Q for the sharp resonance (mode 1) and the broad resonance (mode 2). Spectral response for different radius of the rods of the structure is shown in Fig. 7 (a) and Fig. 7 (b) shows the variation in the quality factor of the device with change in radius of the rods. The radius of the rod has been increased from 0.07μm to 0.11μm in steps of 0.01μm.

From Fig.7 (b) it is seen that for the rods' radius of 0.09 μm, the device exhibits (i) maximum Q and also (ii) maximum difference in Q for mode 1 and mode 2 so we can justify keeping the radius of the PC rods at 0.09μm.

3.3 Performance of the Designed Sensor

To gauge the sensitivity (S) and the FOM of the sensor,shift in the spectral response with change background RI is investigated. The sensitivity and the FOM are calculated as:

$$S = \frac{\Delta\lambda}{\Delta n} \left(\frac{\text{nm}}{\text{RIU}}\right) \quad \ldots (5)$$

$$FOM = \frac{S}{FWHM} (RIU)^{-1} \quad \ldots (6)$$

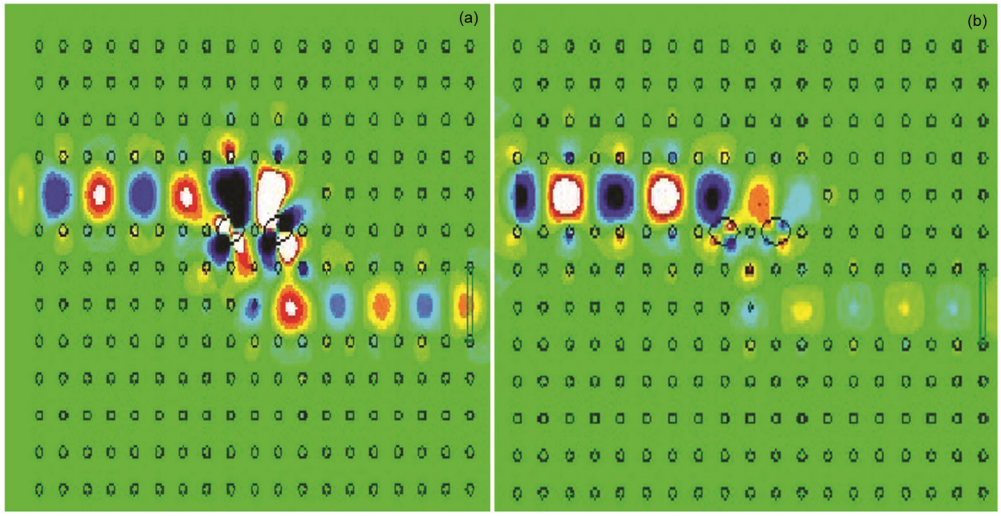

Fig. 5 — Electric field distribution of the device corresponding to the resonant wavelengths (a) λ= 1.5601μm(b) λ=1.5901μm

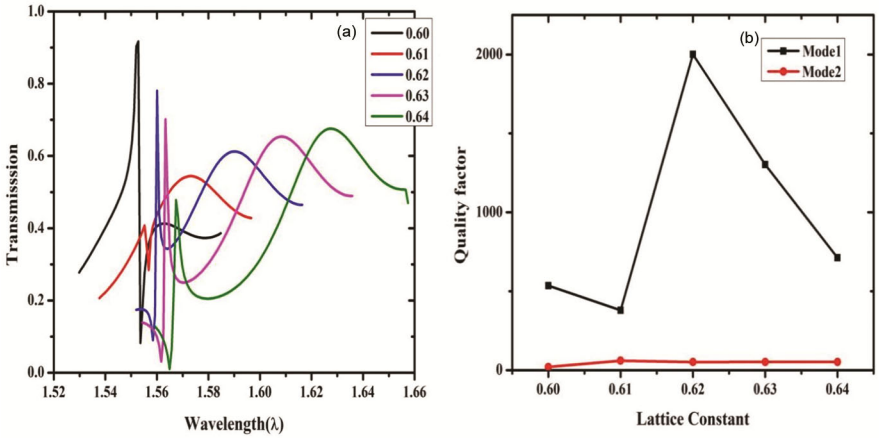

Fig. 6 — (a) Variation of spectral response with different lattice constant (b) Variation of Quality factor with different lattice constants

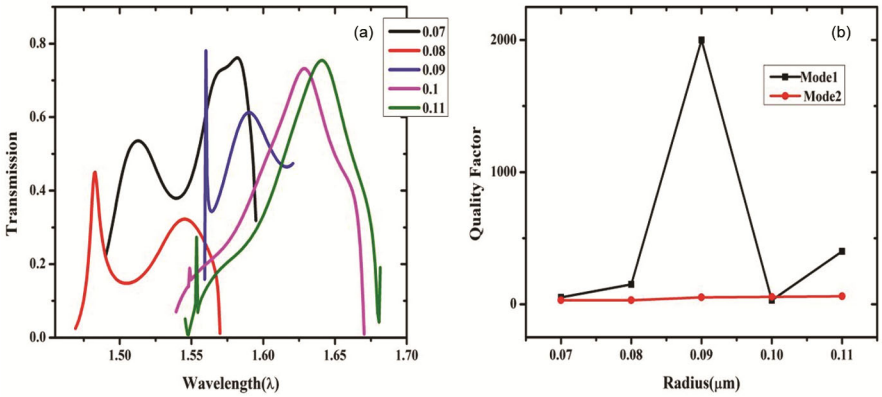

Fig. 7 — (a) Variation of spectral response with different radius of the rods of the proposed structure (b)Variation of quality factor with different radius of the rods of the proposed structure

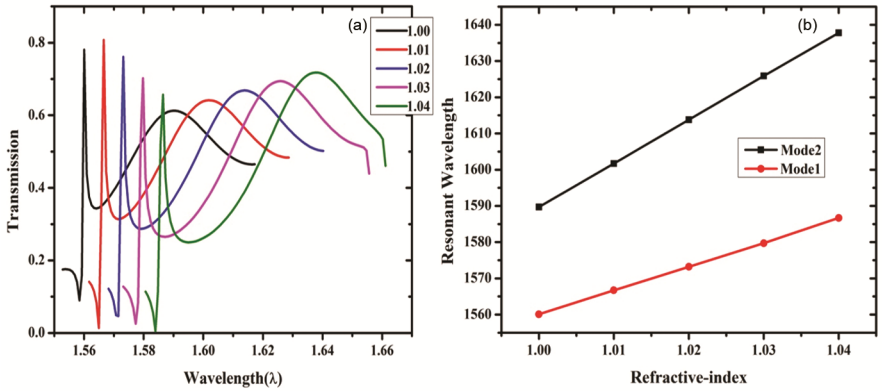

Fig. 8 — (a) Variation of spectral response with background RI (b) Shift of resonant wavelength with background RI

where, the $\Delta\lambda$ is the shift in the wavelength of Fano-type resonance with the variation in RI which is denoted by Δn.

The quality factor (Q) is calculated as: $Q = \frac{\lambda}{FWHM}$

The FWHM is the full width at half maximum. λ is the Fano-type resonant wavelength.

Figure 8 (a) shows the variation of the spectral response of the device with changes in the background RI. It is clear from Fig. 8 (a) that the spectral response shows a drastic red shift in the

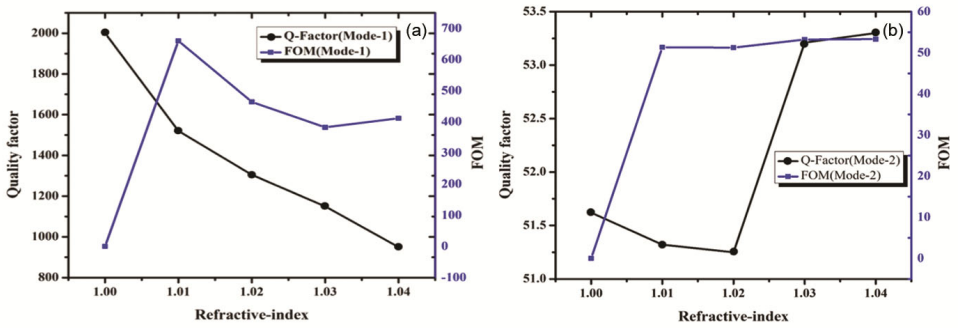

Fig. 9 — (a) Variation of Q and FOM with the background RI in case of Model (b)Variation of Q and FOM with the background RI in case of Mode2

Table 1 — The Comparison of Fano resonance-based RI sensor with existing designs

Reference	Sensitivity (nm/RIU)	Quality Factor	FOM(RIU^{-1})
(22)	1060	-	176.7
(25)	377.2	-	-
(28)	906.9	-	119.7
(29)	657	145	109
(30)	702.35	-	3040.26
(32)	2000 $^{(GH_z}/_{RIU)}$	920	514.40
This Work	1210	2000.5	600

resonant wave length even for a minute (as small as 0.01) change in RI. It is found that mode 1 shows a sensitivity of $700\frac{nm}{RIU}$, While mode 2 shows a sensitivity of $1210\frac{nm}{RIU}$.

It is seen in Fig. 8 (b) that mode 1 and mode 2 both exhibit linear redshift in resonant wavelength with the change in the background RI. We can also see that mode 2 undergoes more shift compared to mode 1.

It is clearly seen in Fig. 9 (a) that the Q of the device gradually decreases with an increase in the background RI. The FOM also shows a slight decrease though not as much as the quality factor under the same condition. Mode 1 exhibits a quality factor of 2000.5 and FOM of 600 RIU^{-1} (Table 1).

From Fig. 9 (b) it can be seen that the change of Q in case of mode 2 is very small as it shows a variation within the range of 51.62 to 53.30 same is the case with FOM as it remains almost constant under the same conditions. Mode2 exhibits a quality factor of 51.32 and an FOM of 53.31.

4 Conclusion

A two dimensional silicon photonic crystal based RI sensor is designed. The spectral response of the device exhibits dual Fano-type (asymmetric) resonance. The device shows a sensitivity of 1210nm/RIU and a maximum quality factor and Figure of merit of 2000.5 and 600 RIU^{-1} respectively. The performance of the designed sensor has been compared with previously proposed RI sensor designs. The size of the sensor is very compact that allows for its on-chip use and can easily be integrated in any system. It is found in the investigations that the structural parameters can be manipulated to exhibit multi-spectral response which forms the basis of further research explorations on the proposed design.

References

1 Johnson S G, Mekis A, Fan S & Jannopoulus J D, *Comput Sci Eng,* 3(6) (2006) 38.
2 Notomi M*, Reports Prog Phys,* 73 (9) (2010) 096501.
3 Medhekar S & Sarkar R K, *Opt Lett*, 30 (8) (2006) 887.
4 Kumar A & Medhekar S, *Opt Laser Tech* 123 (2020) 105910.
5 Rajasekar R & Robinson S, *Plasmonics* 14 (2019) 3.
6 Madhumitha M, Selvendran S, *et.al*., *Optik,* 228 (2021) 166162.
7 Wang S, Cheng Qi, Lv J & Wang J, *J Appl Phy*, 128 (2020) 034501.
8 Sharma P & Medhekar S, *J Opt*, 52 (2022) 504.
9 Wei Fu H, Zhao H, Qiao X, Li Y, Zhao D & Yong Z, *Optoelectron Lett*, 7 (2011) 419.
10 Robinson S & Dhanalaksmi M, *Photonic Sens*, 7 (2017)11.
11 Ge R, Xie J, Yan B, Liu E & Tan W, *JOSA* A, 35 (2018) 992.
12 Qi C, Shutao W, Jiangtao L, Na L & Bo P, *Opt Comm,* 464 (2020) 125393.

13 Mahmoodi Y & Fathi D, *Opt Laser Tech,*138 (2021) 106865.
14 Zaky Z A, Ahamed M A, Shalaby A S & Aly A H, *Sci Rep*, 10 (2020) 9736.
15 Chen J, Gan F, Wang Y & Li G, *Opt Mat*, 6 (2018) 1701152.
16 Huang T, Zeng S, Zaho X, Cheng Z & Shum P P, *Photonics*5 (2018) 23.
17 Yu Y, Heuck M, Hu H, Xue W, Peucheret C, Chen Y, Katsue L, Yvind K & Mork J, *Appl Phys Lett,* 105 (2014) 061117.
18 Rezaei M H & Yaveri M H, *Opt Quant Electron*, 51 (2019) 237.
19 Chen B, Chen B Y, Xia Y, Zhang Y & Fan Li M, *Optoelectron Lett*, 16 (2020) 349.
20 Saudan Q, Bekele D A, Dong G, Yu Y, Yvind K, Mørk J & Galili M, *Opt Exp*, 30 (2022) 7457.
21 Zhan Y, Lei D Y, li X & Maier S A, *Nanoscale,* 6 (2014) 4705.
22 Zafar R & Salim M, *IEEE Sens J,* 15 (2015) 6313.
23 Zhang Y, Liang Z, Meng D, Qin Z, Fan Y, Shi X, Smith D R & Hou E, *Res Phys,* 24 (2021) 1014129.
24 Liu G D, Wang L L, Lin Q, Xia S X, Luo X & Zhao C J, *Plasmonics,* 13 (2018) 15.
25 Wang S, Cheng Qi, Lv J & Wang J, *J Appl Phys*, 128 (2020) 034501.
26 Mohamed Z, Elshahat S, Elnaiem A M A & Almoktar M, *Opt Quantum Electron,* 55 (2023) 943.
27 Kilic S C & Kokaman S, *IEEE Sens J,* 21 (2021) 7551.
28 Shen Z & Du M, *Opt Express,* 29 (2021) 28287.
29 Zhou Y, Guo Z, Zhao X , Wang F, Yu Z, Chen Y, Liu Z, Zhang S, Sun S & Wu X, *Adv Opt Mater,*10 (2022) 2200965.
30 Harhouz A, Tayoub H & Hocini A, *Phys Scr,* 99 (2024) 055545.
31 Wu H & Zhang H, *Appl Opt,* 61 (2022) 10267.
32 Agrawal P, Kishor K & Sinha R K, *IEEE Sens J*, 8 (2024) 3500704.